Journal of Hazardous Materials 260 (2013) 434–441

Contents lists available at SciVerse ScienceDirect

Journal of Hazardous Materials

journal homepage: www.elsevier.com/locate/jhazmat

Photocatalytic generation of multiple ROS types using low-temperature crystallized anodic TiO_2 nanotube arrays

Yulong Liao[a,1], Jonathon Brame[b,1], Wenxiu Que[a,*], Zongming Xiu[b], Haixia Xie[a], Qilin Li[b], Marian Fabian[c,2], Pedro J. Alvarez[b,**]

[a] Electronic Materials Research Laboratory, School of Electronic and Information Engineering, Xi'an Jiaotong University, Xi'an, Shaanxi, China
[b] Department of Civil and Environmental Engineering, Rice University, Houston, TX 77005, USA
[c] Biochemistry and Cell Biology, Rice University, Houston, TX 77005, USA

HIGHLIGHTS

- Low-temperature crystallized TiO_2 nanotubes (LT-NTs) are efficient photocatalysts.
- LT-NTs produce multiple ROS ($^1O_2$ and OH·) while traditional NTs produce no $^1O_2$.
- Crystallization parameters control morphology for potentially tunable photocatalysis.
- Green method to produce immobilized TiO_2 photocatalyst.

ARTICLE INFO

Article history:
Received 10 April 2013
Received in revised form 23 May 2013
Accepted 24 May 2013
Available online xxx

Keywords:
TiO_2
Nanotubes
Photocatalysis
Crystallization
Reactive oxygen species
Green synthesis

ABSTRACT

This study investigates the photocatalytic efficiency, type of reactive oxygen species (ROS) produced, and potential for structural and morphological modification of anodic TiO_2 nanotubes (NTs) synthesized using a novel, energy efficient, low temperature crystallization process. These TiO_2 NTs show greater photocatalytic efficiency than traditional high-temperature sintered NTs or supported Degussa P25 TiO_2, as measured by degradation of methyl orange, a model organic dye pollutant. EPR analysis shows that low-temperature crystallized TiO_2 NTs generate both hydroxyl radicals and singlet oxygen, while high-temperature sintered TiO_2 NTs generate primarily hydroxyl radicals but no singlet oxygen. This "cocktail" of reactive oxygen species, combined with an increased surface area, contributes to the increased efficiency of this photocatalytic material. Furthermore, variation of the NT crystallization parameters enables control of structural and morphological properties so that TiO_2-NTs can be optimized for scale-up and for specific treatment scenarios.

1. Introduction

Titanium dioxide (TiO_2) has been extensively studied as a photocatalyst for advanced oxidation processes to remove hazardous substances from air and water [1–4]. Efficient removal of diverse contaminants such as organic dyes [5–8], endocrine disrupting compounds and pharmaceuticals [9–11], aromatics [12–14], pesticides [15,16], microorganisms [17,18] and heavy metals [19] has made TiO_2 a promising material for multipurpose advanced water treatment systems. Upon illumination, TiO_2 converts incoming photons into excitons, or electron/hole pairs, which can either recombine and dissipate the energy as heat or migrate to the material surface, where they can participate in redox reactions and generate reactive oxygen species (ROS) such as hydroxyl radicals (OH·) and super oxide (O_2^-) [1,20]. These energetic species can further react to form $^1O_2$ and then these ROS contribute to the degradation and removal of unwanted contaminants from water.

While TiO_2 remains the most widely used photocatalyst, the difficulty and energy cost of separating and reusing suspended TiO_2 particles from treated water has increased the interest in immobilized photocatalyst materials [21,22], such as titanium dioxide nanotubes (TiO_2 NTs) [23–26]. TiO_2 NTs offer unique nanotubular structure with high chemical stability, lack of toxicity, and high photochemical activity [27–29]. To date, TiO_2 NTs have been used in numerous applications including photocatalytic treatment of pollutants in air and water [30,31], photovoltaics for energy production [32,33], biomedical applications [34,35], lithium-ion

* Corresponding author. Tel.: +86 029 826687984; fax: +86 029 82668679.
** Corresponding author. Tel.: +1 713 348 5903; fax: +1 713 348 5268.
E-mail addresses: wxque@mail.xjtu.edu.cn (W. Que), fabian@rice.edu (M. Fabian), alvarez@rice.edu (P.J. Alvarez).
[1] Both these authors contributed equally to this work.
[2] Tel.: +1 713 348 4861; fax: +1 713 348 5268.

0304-3894/$ – see front matter © 2013 Elsevier B.V. All rights reserved.
http://dx.doi.org/10.1016/j.jhazmat.2013.05.047

batteries [36,37], water splitting [38–40], and chemical gas sensors [41–43].

Anodization of titanium is the most widely used method for the fabrication of self-organized TiO_2 NT arrays due to ease of control, low cost, and scalable production [44–47]. Anodic TiO_2 NT arrays have shown outstanding photocatalytic performance [30,33], and may be particularly beneficial for photocatalysis due to their large surface area, short diffusion distance between electron/hole generation sites and the material surface (limiting electron/hole recombination), and their inherent immobilization, reducing the energy and material cost of separating the photocatalyst after treatment. However, regardless of their preparation method, anodic TiO_2 NT arrays are always amorphous, necessitating post-fabrication crystallization by heat treatment such as thermal annealing [48–51] or hydrothermal processing [52–54], which require high temperatures (about 450 °C) or special equipment (e.g., pressurized autoclave vessels). Therefore, there is need for less energy-intensive, more affordable and sustainable crystallization methods.

Recently, we reported an alternative and more environmentally friendly method to crystallize amorphous anodic TiO_2 NTs at lower temperatures [55]. Facile and cost-effective, low temperature crystallization provides a new route for crystalline TiO_2 NT production without extra chemical addition, high energy input or special equipment. However, the photocatalytic efficiency of the TiO_2 NTs synthesized by this method has not been carefully evaluated to assess their potential application for treating recalcitrant hazardous substances. In addition, little is known about how different synthesis conditions affect the fundamental material properties of the TiO_2 NTs that determine their photocatalytic efficiency towards chemical contaminant removal.

This paper seeks to advance understanding of the photocatalytic activity and the type of ROS generated by low-temperature crystallized TiO_2 NTs relative to the more traditional and energy-intensive high-temperature sintered TiO_2 NTs, and to determine the effect of synthesis conditions on NT morphology, which could further influence photocatalytic degradation efficiency. Accordingly, we offer novel insight into low-temperature crystallization mechanisms and potential environmental applications.

2. Experimental

2.1. Preparation of TiO_2 NT arrays

TiO_2 NT arrays were synthesized by electrochemical oxidation of titanium sheets as described previously [24]. Briefly, the titanium sheets were oxidized at 60 V for 2 h in a conventional fluorine-containing electrolyte (ethylene glycol containing 0.25 wt.% NH_4F and 1.0 wt.% deionized (DI) water), using a platinum counter electrode [27]. The electrolyte was kept at 7 °C in a cryogenic slot (THJD-2006WY, Tianheng, China) during the synthesis unless otherwise noted. The as-anodized TiO_2 NT array films were thoroughly washed with DI water and ethanol several times. All the reagents were of analytical grade (Sinopharm Group Chemical Reagent Co. Ltd., China).

2.2. Crystallization of the TiO_2 NTs arrays

Two methods were used to crystallize the amorphous anodized TiO_2 NTs: the novel, water-assisted, low temperature (LT) method, and the traditional, high-temperature (HT) method. The LT method used here involved immersing the amorphous TiO_2 NT films in DI water at 90 °C for 10 h, followed by drying in ambient air. The crystallization temperature (70, 90, and 110 °C) and heating duration (10, 20, 24 and 30 h) were then varied to determine their effects on the crystallization process. Aqueous solutions of $CuCl_2$ or $FeCl_3$ were tested as a crystallization medium in place of DI water to investigate the effect of metal ions—which are commonly used as dopants in semiconductor photocatalysis [36,56,57]—on the crystallization process. Experiments above the solvent boiling points were carried out in an autoclave. The HT method involved heating the NT films at 450 °C for 3 h.

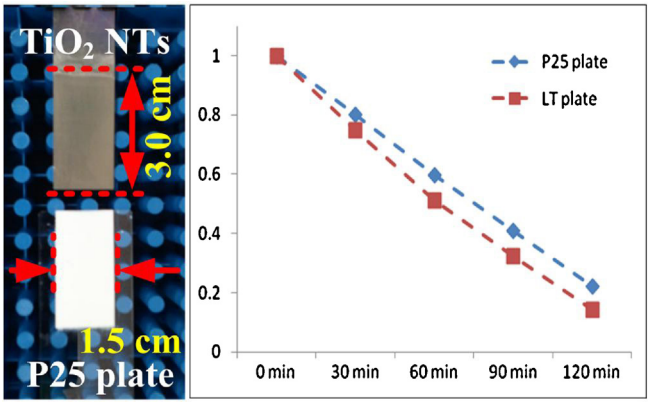

Fig. 1. Digital photographs of P25 plate (left, top) with similar area as the crystallized TiO_2 NT array film (LT plate, left bottom), and corresponding photocatalytic performance in MO degradation. $[MO]_0 = 20$ mM, error bars represent 95% CI and are too small to be seen.

2.3. TiO_2 NT characterization

The crystalline properties of all the samples were characterized by X-ray diffraction as described previously [24], along with transmission electron microscopy (TEM, JEM 2100, JEOL Inc., Japan TEM) and UV-Vis spectrometry (Ultrospec 2100 pro). The Brunauer–Emmett–Teller (BET) surface area was determined by nitrogen adsorption measurement at 77 K (Model ASAP 2020, Micromeritics, USA). TiO_2 NTs were scraped from the Ti metal surface, weighed and measured for BET surface area. All the samples were degassed at 100 °C for 24 h prior to nitrogen adsorption measurement. Photocatalytic ROS production was characterized by electron paramagnetic resonance (EPR) measurement using a Varian E-6 spectrometer under the following conditions: temperature = 293 K; microwave frequency = 9.225 GHz; microwave power = 10 mW; modulation amplitude = 1 G at 100 kHz; and scan time = 4 s. The compounds 2,2,6,6-tetramethyl-4-piperidinol (TMP) [58] and α-(4-pyridyl-1-oxide)-N-*tert*-butylnitrone (POBN) [59] were used as spin-trapping agents for $^1O_2$ and OH·, respectively.

2.4. Photocatalytic and photochemical characterization

The crystallized TiO_2 NT films were tested as photocatalysts, and their photo-activities were evaluated on the basis of the degradation of methyl orange (MO) and 4-chloro-phenol (4CP) as model organic pollutants in aqueous solutions (40 mL total volume, 20 and 100 mM L^{-1}, respectively). The TiO_2 NT films (3.0 cm × 1.5 cm frontal surface area, total mass = 0.04 g) were immersed in the solution and irradiated with six 4-W UV bulbs (Eiko, Black Light Blue, Shawnee, KS; 18 W m^{-2} measured illumination intensity). The photocatalytic activities of NTs sintered for 3 h at high temperature (450 °C) and a similar film of Degussa P25 TiO_2 with the same frontal surface area applied with a razor blade and calcined at 450 °C (Fig. 1) were also compared under identical conditions.

Photodegradation experiments lasted 120 min with 1 mL aliquot samples removed periodically, and were carried out in an open quartz photoreaction vessel with rapid stirring at 23 °C [60]. The pH of the system was neutral (pH 7) throughout the

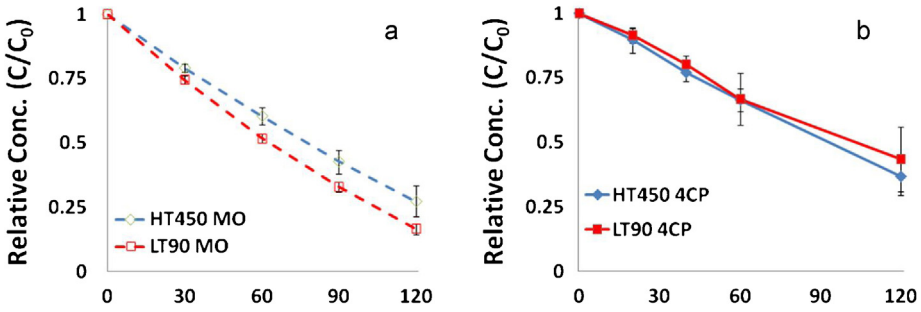

Fig. 2. Photocatalytic performance of traditional high-temperature sintered (HT 450) and low-temperature (LT-90) TiO_2 NT films in degradation of (a) MO, and (b) 4CP. $[MO]_0 = 20$ mM, $[4CP]_0 = 100$ mM, error bars represent 95% CI.

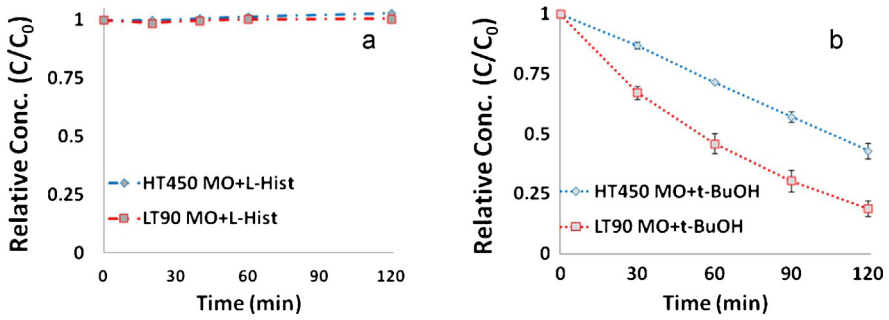

Fig. 3. Photocatalytic performance of traditional high-temperature sintered (HT 450) and low-temperature (LT-90) TiO_2 NT films in degradation of MO with (a) L-histidine as a ROS scavenger, and (d) *tert*-butanol as a OH· scavenger. $[MO]_0 = 20$ mM, $[L\text{-hist}]_0 = [t\text{-BuOH}]_0 = 20$ mM, error bars represent 95% CI.

experiments. The concentration of the residual MO was measured by a UV-Vis spectrometer (Ultrospec 2100 pro), while the concentration of residual 4CP was measured by HPLC (Shimadzu Prominence LC20) with a C18 column and acetonitrile and phosphoric acid (60:40 v:v) as the mobile phase. L-Histidine and *tert*-butanol were used as ROS scavengers at concentrations of 20 mM.

3. Results and discussion

3.1. Photocatalytic activity and ROS production of the low-temperature crystallized TiO_2 NT arrays

TiO_2 NT films were crystallized using both the novel low-temperature, water assisted method (LT-90; heated in water at 90 °C for 20 h) and the traditional high-temperature sintering method (HT-450; heated in air at 450 °C for 3 h). Characterization using both TEM and XRD showed similar TiO_2 peaks consistent with anatase crystalline material, with no other TiO_2 crystal forms (rutile or brookite) observed (Figure S1, ESI). The crystallization mechanism for this low-temperature process was previously hypothesized to follow a traditional dissolution-recrystallization process [61–63], which we confirmed by observing the formation of anatase TiO_2 particles during crystallization (Figure S2, ESI). These NT films were then tested for photocatalytic ROS generation and degradation of several model compounds in water. The LT-90 NTs had higher photocatalytic activity than HT-450 for the degradation of MO (Fig. 2a), and similar photocatalytic activity for the degradation of 4CP (Fig. 2b). The LT-90 NT photocatalytic activity was also compared to a similar plate of Degussa P25 TiO_2, which is the most commonly studied form of TiO_2. LT-90 exhibited higher photocatalytic activity than the P25 loaded on a plate with similar frontal area (Fig. 1). Although using a similar frontal area does not allow for an exact comparison in terms of mass loading or total surface area, it does enable a qualitative evaluation of this novel material in relation to traditional materials. Table 1 summarizes the initial first-order degradation rate constants for the removal of these compounds. Control experiments showed that both direct photolysis and adsorption were negligible (Figure S3, ESI).

The higher degradation efficiency of LT-90 may be partially attributed to its higher specific surface area: 129.0 m^2/g for LT-90 versus 26.8 m^2/g for HT-450 (Figure S4, ESI) and 50.5 m^2/g for commercial P25 TiO_2 [64] (although the BET surface area of the attached P25 TiO_2 was not measured and was likely lower than literature values due to aggregation during the immobilization and annealing process). Although there was no significant adsorption of MO or 4CP onto the NT surface, larger surface area is conducive to increased efficiency due to higher availability of photocatalytic ROS generation sites and greater opportunity for interaction between photo-generated electrons/holes or ROS and contaminants at the photocatalytic surface. Furthermore, TiO_2 NTs offer significant advantages over immobilized P25 TiO_2 in that they do not require an attachment step (saving cost and processing), have a significantly larger surface area, and are less likely to detach during treatment.

To further understand the role of photo-generated ROS, photocatalytic degradation of MO by LT-90 and HT-450 TiO_2 NTs was

Table 1
First order degradation rates.

Material/conditions	1st order degradation rate ($min^{-1} \times 10^{-3} \pm$ standard deviation)
LT-90 + MO	14.7 ± 1.5
HT-450 + MO	10.7 ± 0.8
P25 Plate + MO	12.2 ± 1.4
LT-90 + 4CP	6.7 ± 0.8
HT-450 + 4CP	6.9 ± 0.4
P25 Plate + 4CP	6.6 ± 0.4
LT-90 + MO + t-BuOH	13.8 ± 0.3
HT-450 + MO + t-BuOH	7.0 ± 0.5
P25 Plate + MO + t-BuOH	8.0 ± 0.5

characterized in the presence of two different ROS scavengers at 20 mM: L-histidine (which acts as a global ROS scavenger) and *tert*-butanol (t-BuOH, a preferrential OH· scavenger) [65,66] (Fig. 3). No degradation occurred with LT-90 or HT-450 in the presence of L-histidine (Fig. 3a), which confirms the critical role of ROS in MO degradation. Furthermore, addition of t-BuOH, which helps discern the role of OH· (Fig. 3b), had a greater impact on the degradation of MO by HT-450 (rate constant reduction by 35%, Table 1) than by LT-90 (7% reduction, Table 1). This suggests that OH· mediated degradation plays a more significant role in the presence of HT-450 compared to LT-90, and that other ROS (e.g., $^1O_2$ or O_2^-) or direct electron/hole oxidation also played a role (because degradation was not completely stopped by t-BuOH).

EPR analysis was conducted to further characterize the role of ROS production in TiO_2 NT photocatalytic performance. We used two different spin traps: POBN, which is a general radical trap, and TMP, which acts as a $^1O_2$ trap. When POBN interacts with a radical species such as OH·, it forms a spin adduct, which is much longer lived than the hydroxyl radical (lifetime 5 μs) [20], facilitating measurement. This spin adduct can then be detected by EPR and compared to characteristic radical signatures. The detection of $^1O_2$ is based on oxidation of TMP to 2,2,6,6-tetramethyl-4-piperidinol-*N*-oxyl radical (TMPN), which can be monitored by EPR. Both the LT-90 and the HT-450 NT array films produced characteristic OH· spectra as shown by the POBN response (Fig. 4a), but attempts to isolate O_2^- EPR peaks from the POBN signal using super oxide dismutase as a O_2^- quencher were unsuccessful. Only the LT-90 sample produced $^1O_2$ as shown by the oxidation of TMP to TMPN (Fig. 4b).

There are several possible mechanisms for $^1O_2$ production by TiO_2, including direct photosensitization, ion annihilation and (most commonly) oxidation of superoxide [67–69]. Superoxide is

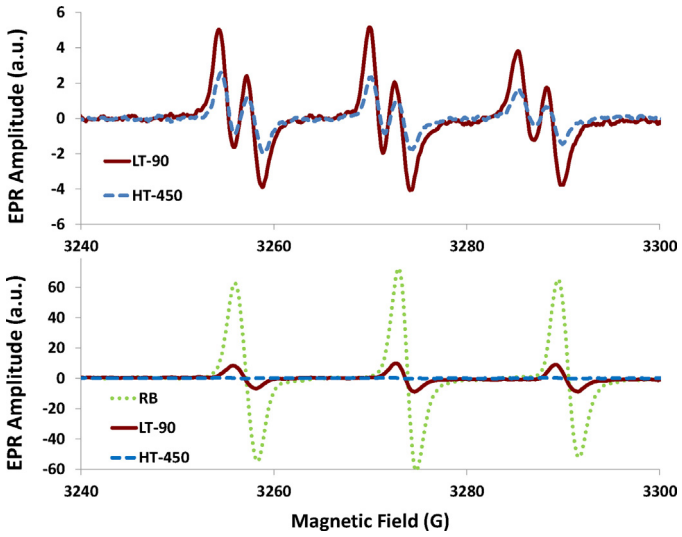

Fig. 4. EPR data showing generation of hydroxyl radicals (OH·) using a POBN trap (a) and singlet oxygen using a TMP trap (b) by illuminated LT-90 and HT-450 photocatalysts. Both photocatalysts produce hydroxyl radicals, while only the LT-90 material produces singlet oxygen ($^1O_2$). Rose Bengal (RB) was used as a positive control for $^1O_2$ production.

commonly formed by an interaction between dissolved oxygen and a photo-generated electron, which can be subsequently oxidized by a photogenerated hole to form $^1O_2$. This process may be facilitated by the smaller crystal size (6–7 nm) of the LT-90 NTs compared to the traditional HT-450 NTs (20–22 nm) according to the Scherrer equation (based on facet (1 0 1) at $2\theta \approx 25.28^\circ$) [52]. While an

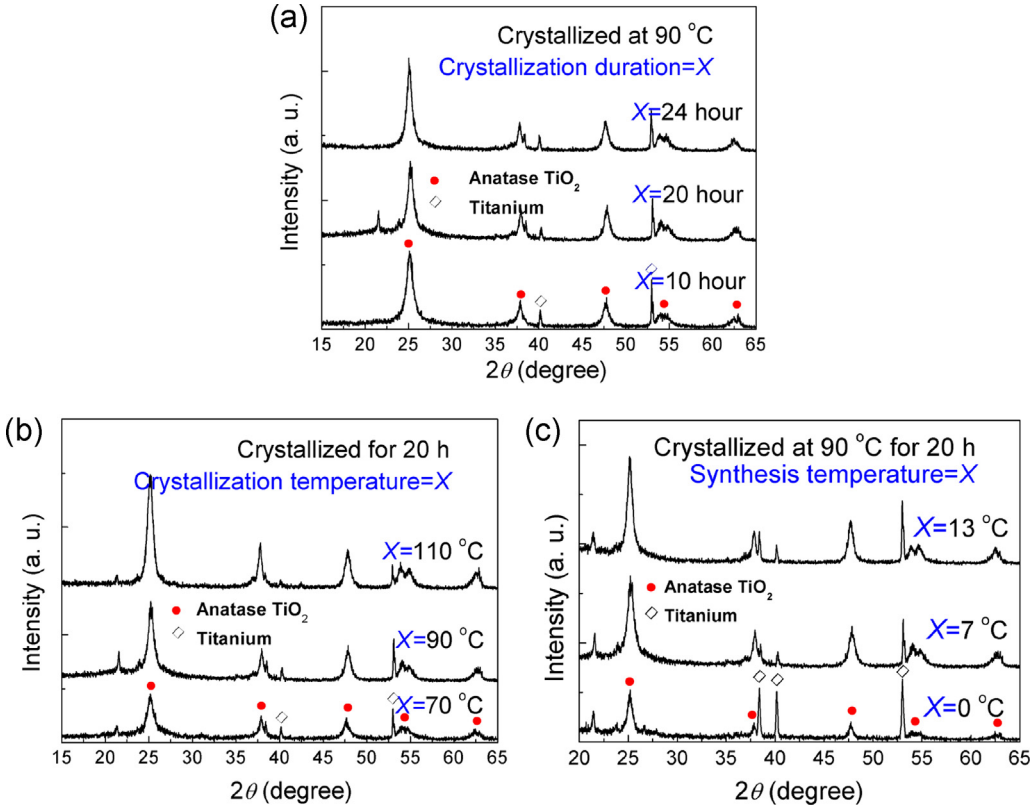

Fig. 5. Crystal diffraction peaks of the anodic TiO_2 NT array films under different conditions: (a) different crystallization durations; (b) different crystallization temperatures; (c) different synthesis temperatures. Desired crystallinity and micro-structure properties of anodic TiO_2 NTs can be achieved by manipulating these parameters.

in-depth exploration of the mechanism of $^1O_2$ production is beyond the scope of this study, it is likely that the smaller crystal size combined with the increased surface area increased the likelihood of superoxide oxidation near the NT surface, thus enabling $^1O_2$ formation. The presence of the TMPN $^1O_2$ signal in the EPR spectra for the LT NT array confirms that low-temperature crystallization produces a photocatalyst that generates both OH· and $^1O_2$, while high temperature sintered TiO_2 NTs generated primarily OH· with no $^1O_2$.

The ability to produce multiple types of ROS could make low-temperature crystallized photocatalysts especially useful for photocatalytic treatment of recalcitrant hazardous substances in natural waters and wastewater effluents. Natural water and wastewater contain significant amounts of background organic matter, while the target hazardous compounds are usually present at trace concentration levels. In such systems, there can be a significant reduction or even complete loss of photocatalytic activity towards the target contaminants due to OH· radical scavenging by the background organic matter [70]. Singlet oxygen, while a weaker oxidant, has been shown to be less impacted by the presence of dissolved organic matter [71]. While ROS generation by photocatalytic materials has been extensively studied, little has been reported about the effect of multiple ROS or the impact of a combination of ROS on contaminant degradation [72]. This generation of multiple types of ROS could be beneficial for treatment of mixtures of emerging pollutants and other recalcitrant hazardous organics, although the extent to which low-temperature crystallized TiO_2 NTs enhance the range of contaminants removed from complex mixtures remains to be determined.

3.2. Influence of crystallization conditions on TiO_2 NT material properties

To provide insight for the optimization and scale-up of low-temperature crystallized NTs and to further understand the impact of various experimental conditions on the morphology and other physical properties of these materials (which control their photocatalytic performance) the amorphous anodic TiO_2 NT films were treated in water under a series of controlled conditions.

The crystallization heating time was varied to help optimize energy use and determine the effect of heating time on crystal structure. Fig. 5a shows that the TiO_2 NT samples heated at 90 °C for 10, 20 and 24 h exhibit similar XRD patterns, all crystallized to anatase. The degree of crystallinity and the crystal size increase slightly with increasing heating time. Since only crystalline TiO_2 is capable of photocatalytic degradation, a higher degree of crystallinity may increase degradation efficiency, while crystal size may be important in the production of $^1O_2$ as previously discussed. However, excess heating (30 h) in water resulted in the peeling of TiO_2 NTs from the Ti substrate (Figure S5, ESI).

The morphological properties of the TiO_2 NTs before and after crystallization (at 90 °C) were characterized by field emission-scanning electron microscopy (FE-SEM) (Fig. 6). Before crystallization, the as-anodized TiO_2 NT arrays were open, with an

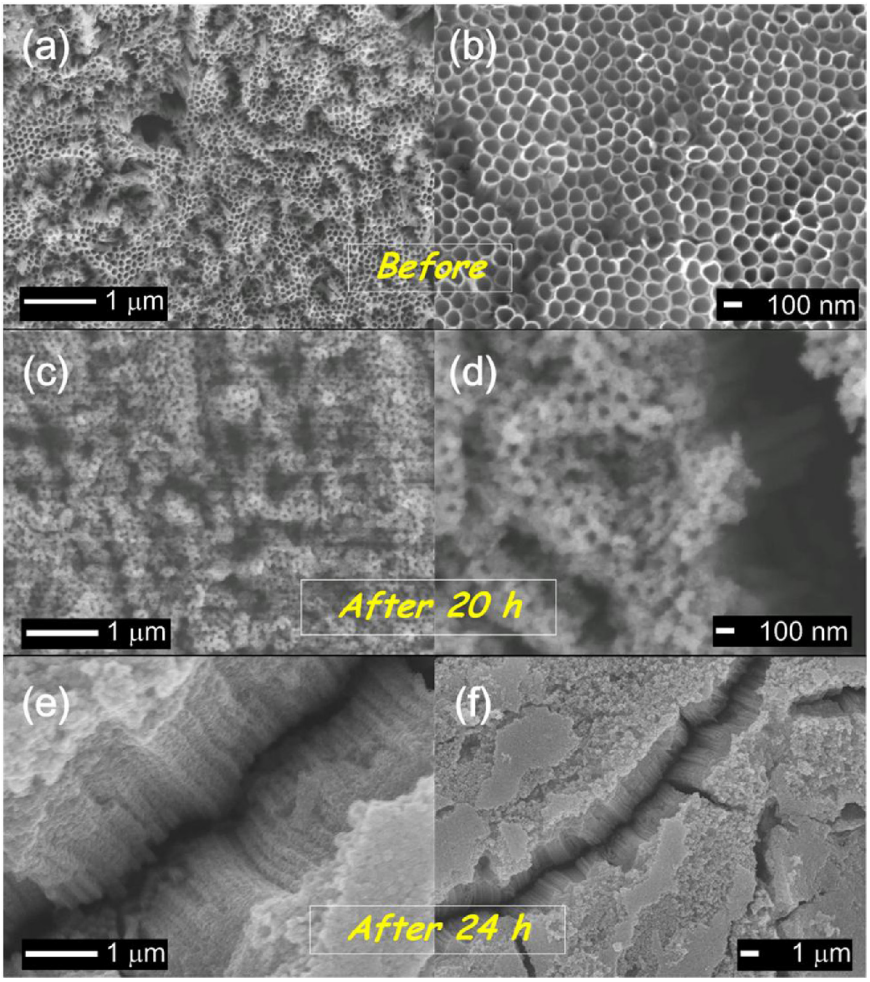

Fig. 6. SEM images of the anodic TiO_2 NT array films showing the morphology before and after water treatment at 90 °C. Desired crystallinity and micro-structure properties of anodic TiO_2 NTs can be achieved by manipulating the treatment parameters.

inner diameter of 100 nm and a wall thickness of 10 nm (Fig. 6a and b). After heating in water for 20 h, the tubular structure of the TiO_2 NTs was maintained, but the inner diameter decreased to 30 nm, the tube wall thickness increased up to 80 nm, and the surface appeared rougher (Fig. 6c and d). This suggests less dense, possibly porous walls. A rougher morphology provides more active surface sites, which is beneficial for photocatalysis (e.g., surface reaction area, electron charge transfer paths) as well as other applications (e.g., sensors, solar cells) [28]. However, after the heating time increased to 24 h, the one-dimensional tube structure was lost, and cracks appeared on the TiO_2 NT film, which could be problematic for some applications.

In traditional sintering, an increased crystallization temperature can result in different crystal phases (e.g., rutile, brookite) [48–50]. To determine if there is a similar change in crystal structure using this low-temperature method, the crystallization temperature was varied. Fig. 5b shows that amorphous anodic TiO_2 NTs are efficiently crystallized into the anatase phase in water at a wide range of temperatures from 70 to 110 °C, with crystal size increasing with increased temperature. However, the TiO_2 NTs detached from the Ti substrate when treated at 110 °C for 20 h, and no other TiO_2 crystal structure was observed. FE-SEM images show that the nanotubular structure disappeared after only 3 h of treatment at 110 °C (Figure S6, ESI), which may be attributed to the special hydrothermal environment used in an autoclave to achieve water heating at 110 °C. In contrast, at both 90 and 70 °C, crystallinity and firm attachment to the substrate were achieved. Disorientation (loss of NT alignment) and detachment of nanotubes from the underlying substrate has been a severe limitation for traditional solvothermal or hydrothermal crystallization methods for years [27]. This water-assisted low-temperature crystallization method at temperatures below 110 °C offers an effective solution to this problem.

Fig. 5c shows the crystallization of TiO_2 NTs that were synthesized under different NT anodic growth temperatures (0 °C, 7 °C, 13 °C). After being treated in water at 90 °C for 20 h, they exhibited similar XRD patterns, indicating that all the TiO_2 NTs were crystallized into the anatase phase. Furthermore, the intensity of the primary anatase (1 0 1) peak at 25.28° increased with the anodic synthesis temperature, indicating the presence of more crystalline material. As previously reported, higher synthesis temperature produces longer tubes [44,47]. Since the longer tubes (those with higher synthesis temperatures) also have more crystalline material, we infer that crystallization of the anodic TiO_2 NTs occurs throughout the tube length, which could increase the active surface area for photocatalytic ROS generation and may contribute to the observed increase in degradation rate.

The effect of metal ions in the crystallization medium was also tested to determine if the crystal structure of the TiO_2 can be altered during crystallization, since metal-ion doping is a common means of altering the photo-physical properties of semiconductor photocatalysts [73]. The presence of metal ions in the heating water with a charge-to-size ratio similar to titanium disrupted the TiO_2 crystallization process. Fig. 7 shows the crystal structure of the anodized TiO_2 NTs crystallized in Cu^{2+} and Fe^{3+} aqueous solution (0–1 M, at 90 °C for 10 h). Cu^{2+}, which has a significantly smaller charge to size ratio than Ti (i.e., 27 versus 66 charge/nm) had no apparent effect on crystallization (Fig. 7a). In contrast, Fe^{3+} (46 charge/nm) disrupted the crystallization of amorphous TiO_2 NTs into anatase TiO_2, yielding a crystal composite of Ti, Fe and O, containing primarily $Fe_4(TiO_4)_3$ and $Fe_2Ti_3O_9$ peaks identified by reference to the JCPDS database (Fig. 7b). This alternate crystal structure was likely formed when iron cations replaced titanium cations during the dissolution-recrystallization process due to the similar atomic diameters and charge-to-size ratios of iron and titanium (Figure S7, ESI) [74–76]. These results suggest that it may be possible to use

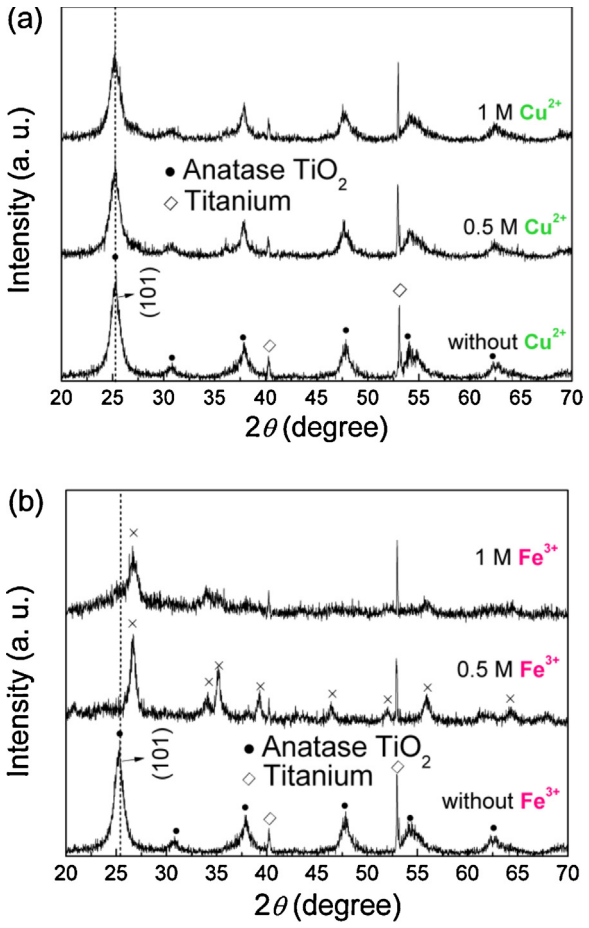

Fig. 7. Crystal diffraction patterns of the anodic TiO_2 NT array films crystallized in the presence of Cu^{2+} (a) and Fe^{3+} (b) in water at 90 °C for 10 h. Dashed lines indicate the location of anatase (1 0 1) peak at $2\theta \approx 25.28°$. The new peak formed at 0.5 M and 1 M Fe^{3+} is indicative of a new Fe–Ti–O crystal species resulting from substitution of Fe^{3+} ions in the place of Ti^{4+} ions in the lattice structure due to their similar charge/size ratio.

ionic crystallization water to dope TiO_2 NTs, enabling visible-light sensitivity for photocatalytic degradation [77].

In summary, anodic TiO_2 NTs can be efficiently crystallized into anatase after heating in water at temperatures from 70 to 90 °C and heating durations of 10–20 h. These parameters, along with synthesis temperature, could be used to selectively control the degree of crystallinity, tube length, micro-structure, and chemical composition of anodic TiO_2 NTs to maximize photocatalytic ROS production efficiency and control the type of ROS produced. Further work is needed to determine the role that each of these morphological properties play in ROS generation type and quantity.

4. Conclusions

Water-assisted crystallization is a green alternative synthesis method for making anatase TiO_2 NTs for potential use as a supported photocatalyst material for advanced oxidation of hazardous organic materials. When used as a photocatalytic material, low-temperature crystallized NTs produce various types of ROS, including hydroxyl radicals and singlet oxygen, which could be particularly useful for photocatalytic treatment of emerging pollutants in complex water matrices such as waste-water treatment plant effluents. This ability to produce multiple ROS was not observed with NTs crystallized by traditional high-temperature sintering, indicating an advantage of the low-temperature crystallization process. Furthermore, the NT synthesis and crystallization parameters

can be varied with the potential for controlled manipulation of crystal and chemical properties such as tube length, interstitial dopants, surface area and crystal size, enabling application-specific optimization. With these remarkable properties, combined with larger surface area, low temperature, water-assisted crystallized TiO_2 NTs are a promising alternative to traditional photocatalytic materials for advanced water and wastewater treatment.

Acknowledgements

We thank Dr. Qingbo Zhang (Rice University) for assistance with TEM. This work was supported by the National Natural Science Foundation of China under Grant Nos. 90923012 and 61078058, and the Science and Technology Developing Project of Shaanxi Province (2012KW-11).

Appendix A. Supplementary data

Supplementary data associated with this article can be found, in the online version, at http://dx.doi.org/10.1016/j.jhazmat.2013.05.047.

References

[1] M.R. Hoffmann, S.T. Martin, W. Choi, D.W. Bahnemann, Environmental applications of semiconductor photocatalysis, Chem. Rev. 95 (1995) 69–96.
[2] A. Mills, S. LeHunte, An overview of semiconductor photocatalysis, J. Photochem. Photobiol. A-Chem. 108 (1997) 1–35.
[3] A. Fujishima, X. Zhang, D.A. Tryk, TiO_2 photocatalysis and related surface phenomena, Surf. Sci. Rep. 63 (2008) 515–582.
[4] H. Choi, E. Stathatos, D.D. Dionysiou, Photocatalytic TiO_2 films and membranes for the development of efficient wastewater treatment and reuse systems, Desalination 202 (2007) 199–206.
[5] I.K. Konstantinou, T.A. Albanis, TiO_2-assisted photocatalytic degradation of azo dyes in aqueous solution: kinetic and mechanistic investigations – a review, Appl. Catal. B-Environ. 49 (2004) 1–14.
[6] B. Neppolian, H.C. Choi, S. Sakthivel, B. Arabindoo, V. Murugesan, Solar/UV-induced photocatalytic degradation of three commercial textile dyes, J. Hazard. Mater. 89 (2002) 303–317.
[7] S.K. Kansal, M. Singh, D. Sud, Studies on photodegradation of two commercial dyes in aqueous phase using different photocatalysts, J. Hazard. Mater. 141 (2007) 581–590.
[8] U.G. Akpan, B.H. Hameed, Parameters affecting the photocatalytic degradation of dyes using TiO_2-based photocatalysts: a review, J. Hazard. Mater. 170 (2009) 520–529.
[9] Y. Ohko, I. Ando, C. Niwa, T. Tatsuma, T. Yamamura, T. Nakashima, Y. Kubota, A. Fujishima, Degradation of bisphenol A in water by TiO_2 photocatalyst, Environ. Sci. Technol 35 (2001) 2365–2368.
[10] R. Thiruvenkatachari, T.O. Kwon, J.C. Jun, S. Balaji, M. Matheswaran, I.S. Moon, Application of several advanced oxidation processes for the destruction of terephthalic acid (TPA), J. Hazard. Mater. 142 (2007) 308–314.
[11] W.T. Tsai, M.K. Lee, T.Y. Su, Y.M. Chang, Photodegradation of bisphenol-A in a batch TiO_2 suspension reactor, J. Hazard. Mater. 168 (2009) 269–275.
[12] U.I. Gaya, A.H. Abdullah, Heterogeneous photocatalytic degradation of organic contaminants over titanium dioxide: a review of fundamentals, progress and problems, J. Photochem. Photobiol. C-Photochem. Rev. 9 (2008) 1–12.
[13] G. Busca, S. Berardinelli, C. Resini, L. Arrighi, Technologies for the removal of phenol from fluid streams: a short review of recent developments, J. Hazard. Mater. 160 (2008) 265–288.
[14] K. Okamoto, Y. Yamamoto, H. Tanaka, M. Tanaka, A. Itaya, Heterogeneous photocatalytic decomposition of phenol over TiO_2 powder, Bull. Chem. Soc. Jpn. 58 (1985) 2015–2022.
[15] I. Oller, W. Gernjak, M.I. Maldonado, L.A. Perez-Estrada, J.A. Sanchez-Perez, S. Malato, Solar photocatalytic degradation of some hazardous water-soluble pesticides at pilot-plant scale, J. Hazard. Mater. 138 (2006) 507–517.
[16] S. Rabindranathan, S. Devipriya, S. Yesodharan, Photocatalytic degradation of phosphamidon on semiconductor oxides, J. Hazard. Mater. 102 (2003) 217–229.
[17] G.K. Prasad, G.S. Agarwal, B. Singh, G.P. Rai, R. Vijayaraghavan, Photocatalytic inactivation of *Bacillus anthracis* by titania nanomaterials, J. Hazard. Mater. 165 (2009) 506–510.
[18] P.K.J. Robertson, J.M.C. Robertson, D.W. Bahnemann, Removal of microorganisms and their chemical metabolites from water using semiconductor photocatalysis, J. Hazard. Mater. 211 (2012) 161–171.
[19] X.H. Guan, J.S. Du, X.G. Meng, Y.K. Sun, B. Sun, Q.H. Hu, Application of titanium dioxide in arsenic removal from water: a review, J. Hazard. Mater. 215 (2012) 1–16.
[20] A.L. Linsebigler, G.Q. Lu, J.T. Yates, Photoctalysis on TiO_2 surfaces: principles, mechanisms, and selected results, Chem. Rev. 95 (1995) 735–758.
[21] G. Balasubramanian, D.D. Dionysiou, M.T. Suidan, I. Baudin, J.M. Laîné, Evaluating the activities of immobilized TiO_2 powder films for the photocatalytic degradation of organic contaminants in water, Appl. Catal. B: Environ. 47 (2004) 73–84.
[22] Y. Chen, D.D. Dionysiou, TiO_2 photocatalytic films on stainless steel: the role of Degussa P-25 in modified sol–gel methods, Appl. Catal. B: Environ. 62 (2006) 255–264.
[23] Y. Liao, W. Que, Q. Jia, Y. He, J. Zhang, P. Zhong, Controllable synthesis of brookite/anatase/rutile TiO_2 nanocomposites and single-crystalline rutile nanorods array, J. Mater. Chem. 22 (2012) 7937–7944.
[24] Y. Liao, W. Que, J. Zhang, P. Zhong, Y. He, A facile method for rapid preparation of individual titania nanotube powders by a two-step process, Mater. Res. Bull. 46 (2011) 478–482.
[25] G. Mascolo, R. Comparelli, M.L. Curri, G. Lovecchio, A. Lopez, A. Agostiano, Photocatalytic degradation of methyl red by TiO_2: comparison of the efficiency of immobilized nanoparticles versus conventional suspended catalyst, J. Hazard. Mater. 142 (2007) 130–137.
[26] Y. Li, X. Zhou, W. Chen, L. Li, M. Zen, S. Qin, S. Sun, Photodecolorization of Rhodamine B on tungsten-doped TiO_2/activated carbon under visible-light irradiation, J. Hazard. Mater. 227–228 (2012) 25–33.
[27] C.A. Grimes, G.K. Mor, TiO_2 Nanotube Arrays: Synthesis, Properties, and Applications, Springer, Dordrecht/Heidelberg/London/New York, 2009.
[28] G.R. Patzke, Y. Zhou, R. Kontic, F. Conrad, Oxide nanomaterials: synthetic developments, mechanistic studies, and technological innovations, Angew. Chem. 50 (2011) 826–859.
[29] D.V. Bavykin, J.M. Friedrich, F.C. Walsh, Protonated titanates and TiO_2 nanostructured materials: synthesis, properties, and applications, Adv. Mater. 18 (2006) 2807–2824.
[30] J.M. Macak, M. Zlamal, J. Krysa, P. Schmuki, Self-organized TiO_2 nanotube layers as highly efficient photocatalysts, Small 3 (2007) 300–304.
[31] K. Woan, G. Pyrgiotakis, W. Sigmund, Photocatalytic carbon-nanotube-TiO_2 composites, Adv. Mater. 21 (2009) 2233–2239.
[32] V. Galstyan, A. Vomiero, I. Concina, A. Braga, M. Brisotto, E. Bontempi, G. Faglia, G. Sberveglieri, Solar cells vertically aligned TiO_2 nanotubes on plastic substrates for flexible solar cells, Small 7 (2011), 2405-2405.
[33] X. Xu, X. Fang, T. Zhai, H. Zeng, B. Liu, X. Hu, Y. Bando, D. Golberg, Nanotubes: tube-in-tube TiO_2 nanotubes with porous walls: fabrication, formation mechanism, and photocatalytic properties, Small 7 (2011), 444-444.
[34] S.Q. Liu, A.C. Chen, Coadsorption of horseradish peroxidase with thionine on TiO_2: nanotubes for biosensing, Langmuir 21 (2005) 8409–8413.
[35] J. Park, S. Bauer, A. Pittrof, M.S. Killian, P. Schmuki, K. von der Mark, Synergistic control of mesenchymal stem cell differentiation by nanoscale surface geometry and immobilized growth factors on TiO_2 nanotubes, Small 8 (2012) 98–107.
[36] L. Xue, Z. Wei, R. Li, J. Liu, T. Huang, A. Yu, Design and synthesis of Cu_6Sn_5-coated TiO_2 nanotube arrays as anode material for lithium ion batteries, J. Mater. Chem. 21 (2011) 3216–3220.
[37] I. Paramasivam, H. Jha, N. Liu, P. Schmuki, A review of photocatalysis using self-organized TiO_2 nanotubes and other ordered oxide nanostructures, Small 8 (2012) 3073–3103.
[38] M.A. Khan, M.S. Akhtar, S.I. Woo, O.B. Yang, Enhanced photoresponse under visible light in Pt ionized TiO_2 nanotube for the photocatalytic splitting of water, Catal. Commun. 10 (2008) 1–5.
[39] C. Cheng, S.K. Karuturi, L. Liu, J. Liu, H. Li, L.T. Su, A.I.Y. Tok, H.J. Fan, Quantum-dot-sensitized TiO_2 inverse opals for photoelectrochemical hydrogen generation, Small 8 (2012) 37–42.
[40] Z. Yin, Z. Wang, Y. Du, X. Qi, Y. Huang, C. Xue, H. Zhang, Full solution-processed synthesis of all metal oxide-based tree-like heterostructures on fluorine-doped tin oxide for water splitting, Adv. Mater. 24 (2012) 5374–5378.
[41] E. Sennik, Z. Colak, N. Kilinc, Z.Z. Ozturk, Synthesis of highly-ordered TiO_2 nanotubes for a hydrogen sensor, Int. J. Hydrogen Energ. 35 (2010) 4420–4427.
[42] Y.-Y. Song, P. Schmuki, Modulated TiO_2 nanotube stacks and their use in interference sensors, Electrochem. Commun. 12 (2010) 579–582.
[43] Q. Zheng, B. Zhou, J. Bai, L. Li, Z. Jin, J. Zhang, J. Li, Y. Liu, W. Cai, X. Zhu, Self-organized TiO_2 nanotube array sensor for the determination of chemical oxygen demand, Adv. Mater. 20 (2008) 1044–1049.
[44] C.A. Grimes, Synthesis and application of highly ordered arrays of TiO_2 nanotubes, J. Mater. Chem. 17 (2007) 1451–1457.
[45] J.M. Macak, H. Tsuchiya, P. Schmuki, High-aspect-ratio TiO_2 nanotubes by anodization of titanium, Angew. Chem. Int. Ed. 44 (2005) 2100–2102.
[46] G.K. Mor, O.K. Varghese, M. Paulose, C.A. Grimes, Transparent highly ordered TiO_2 nanotube arrays via anodization of titanium thin films, Adv. Funct. Mater. 15 (2005) 1291–1296.
[47] H.E. Prakasam, K. Shankar, M. Paulose, O.K. Varghese, C.A. Grimes, A new benchmark for TiO_2 nanotube array growth by anodization, J. Phys. Chem. C 111 (2007) 7235–7241.
[48] N.K. Allam, C.A. Grimes, Effect of rapid infrared annealing on the photoelectrochemical properties of anodically fabricated TiO_2 nanotube arrays, J. Phys. Chem. C 113 (2009) 7996–7999.
[49] Y. Sun, K. Yan, G. Wang, W. Guo, T. Ma, Effect of annealing temperature on the hydrogen production of TiO_2 nanotube arrays in a two-compartment photoelectrochemical cell, J. Phys. Chem. C 115 (2011) 12844–12849.
[50] O.K. Varghese, D. Gong, M. Paulose, C.A. Grimes, E.C. Dickey, Crystallization and high-temperature structural stability of titanium oxide nanotube arrays, J. Mater. Res. 18 (2003) 156–165.

[51] K. Zhu, N.R. Neale, A. Miedaner, A.J. Frank, Enhanced charge-collection efficiencies and light scattering in dye-sensitized solar cells using oriented TiO_2 nanotubes arrays, Nano Lett. 7 (2006) 69–74.
[52] H. Yin, Y. Wada, T. Kitamura, S. Kambe, S. Murasawa, H. Mori, T. Sakata, S. Yanagida, Hydrothermal synthesis of nanosized anatase and rutile TiO_2 using amorphous phase TiO_2, J. Mater. Chem. 11 (2001) 1694–1703.
[53] D.V. Bavykin, V.N. Parmon, A.A. Lapkin, F.C. Walsh, The effect of hydrothermal conditions on the mesoporous structure of TiO_2 nanotubes, J. Mater. Chem. 14 (2004) 3370–3377.
[54] B.D. Yao, Y.F. Chan, X.Y. Zhang, W.F. Zhang, Z.Y. Yang, N. Wang, Formation mechanism of TiO_2 nanotubes, Appl. Phys. Lett. 82 (2003) 281–283.
[55] Y. Liao, W. Que, P. Zhong, J. Zhang, Y. He, A facile method to crystallize amorphous anodized TiO(2) nanotubes at low temperature, ACS Appl. Mater. Interfaces 3 (2011) 2800–2804.
[56] C.Y. Wang, C. Bottcher, D.W. Bahnemann, J.K. Dohrmann, In situ electron microscopy investigation of Fe(III)-doped TiO_2 nanoparticles in an aqueous environment, J. Nanopart. Res. 6 (2004) 119–122.
[57] B. Liu, X. Wang, G. Cai, L. Wen, Y. Song, X. Zhao, Low temperature fabrication of V-doped TiO_2 nanoparticles, structure and photocatalytic studies, J. Hazard. Mater. 169 (2009) 1112–1118.
[58] J. Lee, Y. Mackeyev, M. Cho, D. Li, J.-H. Kim, L.J. Wilson, P.J.J. Alvarez, Photochemical and antimicrobial properties of novel C60 derivatives in aqueous systems, Environ. Sci. Technol. 43 (2009) 6604–6610.
[59] S.G. Huling, R.G. Arnold, R.A. Sierka, M.R. Miller, Measurement of hydroxyl radical activity in a soil slurry using the spin trap α-(4-pyridyl-1-oxide)-N-tert-butylnitrone, Environ. Sci. Technol. 32 (1998) 3436–3441.
[60] J.A. Brame, S.W. Hong, J. Lee, S.-H. Lee, P.J.J. Alvarez, Photocatalytic pre-treatment with food-grade TiO_2 increases the bioavailability and bioremediation potential of weathered oil from the Deepwater Horizon oil spill in the Gulf of Mexico, Chemosphere 90 (2013) 2315–2319.
[61] Y. Liao, W. Que, P. Zhong, J. Zhang, Y. He, A facile method to crystallize amorphous anodized TiO_2 nanotubes at low temperature, ACS Appl. Mater. Interfaces 3 (2011) 2800–2804.
[62] D. Wang, L. Liu, F. Zhang, K. Tao, E. Pippel, K. Domen, Spontaneous phase and morphology transformations of anodized titania nanotubes induced by water at room temperature, Nano Lett. 11 (2011) 3649–3655.
[63] K. Huo, H. Wang, X. Zhang, Y. Cao, P.K. Chu, Heterostructured TiO_2 nanoparticles/nanotube arrays: in situ formation from amorphous TiO_2 nanotube arrays in water and enhanced photocatalytic activity, ChemPlusChem 77 (2012) 323–329.
[64] S. Sakthivel, B. Neppolian, M.V. Shankar, B. Arabindoo, M. Palanichamy, V. Murugesan, Solar photocatalytic degradation of azo dye: comparison of photocatalytic efficiency of ZnO and TiO_2, Sol. Energy Mater. Sol. Cells 77 (2003) 65–82.
[65] R. Zamora, M. Alaiz, F.J. Hidalgo, Feed-back inhibition of oxidative stress by oxidized lipid/amino acid reaction products, Biochemistry-us 36 (1997) 15765–15771.
[66] B.B. Fischer, A. Krieger-Liszkay, R.I.L. Eggen, Photosensitizers neutral red (Type I) and rose Bengal (Type II) cause light-dependent toxicity in *Chlamydomonas reinhardtii* and induce the Gpxh gene via increased singlet oxygen formation, Environ. Sci. Technol. 38 (2004) 6307–6313.
[67] R. Konaka, E. Kasahara, W.C. Dunlap, Y. Yamamoto, K.C. Chien, M. Inoue, Irradiation of titanium dioxide generates both singlet oxygen and superoxide anion, Free Radic. Biol. Med. 27 (1999) 294–300.
[68] Y. Nosaka, T. Daimon, A.Y. Nosaka, Y. Murakami, Singlet oxygen formation in photocatalytic TiO_2 aqueous suspension, Phys. Chem. Chem. Phys. 6 (2004) 2917–2918.
[69] T. Daimon, Y. Nosaka, Formation and behavior of singlet molecular oxygen in TiO_2 photocatalysis studied by detection of near-infrared phosphorescence, J. Phys. Chem. C 111 (2007) 4420–4424.
[70] D. Avisar, I. Horovitz, L. Lozzi, F. Ruggieri, M. Baker, M.-L. Abel, H. Mamane, Impact of water quality on removal of carbamazepine in natural waters by N-doped TiO_2 photo-catalytic thin film surfaces, J. Hazard. Mater. 244–245 (2013) 463–471.
[71] H. Kim, W. Kim, Y. Mackeyev, G.-S. Lee, H.-J. Kim, T. Tachikawa, S. Hong, S. Lee, J. Kim, L.J. Wilson, T. Majima, P.J.J. Alvarez, W. Choi, J. Lee, Selective oxidative degradation of organic pollutants by singlet oxygen-mediated photosensitization: tin porphyrin versus C60 aminofullerene systems, Environ. Sci. Technol. 46 (2012) 9606–9613.
[72] Y. Li, W. Zhang, J. Niu, Y. Chen, Mechanism of photogenerated reactive oxygen species and correlation with the antibacterial properties of engineered metal-oxide nanoparticles, ACS Nano 6 (2012) 5164–5173.
[73] W. Choi, A. Termin, M.R. Hoffmann, The role of metal ion dopants in quantum-sized TiO_2: correlation between photoreactivity and charge carrier recombination dynamics, J. Phys. Chem. 98 (1994) 13669–13679.
[74] H.G. Yang, G. Liu, S.Z. Qiao, C.H. Sun, Y.G. Jin, S.C. Smith, J. Zou, H.M. Cheng, G.Q. Lu, Solvothermal synthesis and photoreactivity of anatase TiO_2 nanosheets with dominant {0 0 1} facets, J. Am. Chem. Soc. 131 (2009) 4078–4083.
[75] S. Yin, Y. Aita, M. Komatsu, J.S. Wang, Q. Tang, T. Sato, Synthesis of excellent visible-light responsive $TiO_{2-x}N_y$ photocatalyst by a homogeneous precipitation-solvothermal process, J. Mater. Chem. 15 (2005) 674–682.
[76] J.C. Yu, L. Wu, J. Lin, P.S. Li, Q. Li, Microemulsion-mediated solvothermal synthesis of nanosized CdS-sensitized TiO_2 crystalline photocatalyst, Chem. Commun. (2003) 1552–1553.
[77] J.H. Park, S. Kim, A.J. Bard, Novel carbon-doped TiO_2 nanotube arrays with high aspect ratios for efficient solar water splitting, Nano Lett. 6 (2005) 24–28.